

Lab on a Chip

Accepted Manuscript



This is an *Accepted Manuscript*, which has been through the Royal Society of Chemistry peer review process and has been accepted for publication.

Accepted Manuscripts are published online shortly after acceptance, before technical editing, formatting and proof reading. Using this free service, authors can make their results available to the community, in citable form, before we publish the edited article. We will replace this *Accepted Manuscript* with the edited and formatted *Advance Article* as soon as it is available.

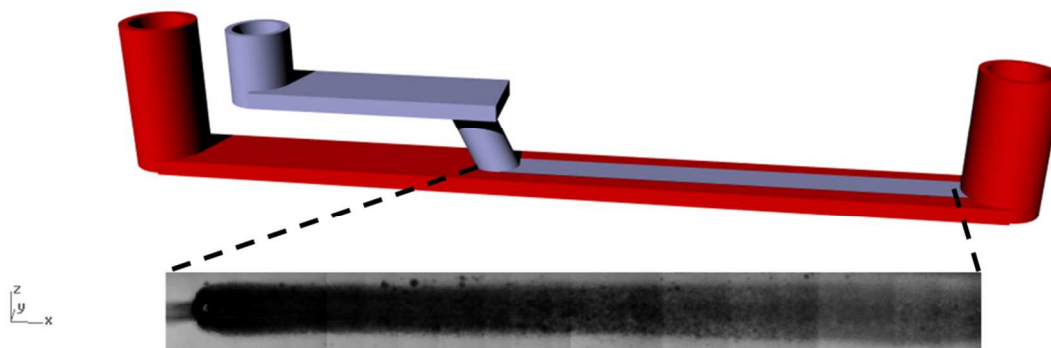
You can find more information about *Accepted Manuscripts* in the [Information for Authors](#).

Please note that technical editing may introduce minor changes to the text and/or graphics, which may alter content. The journal's standard [Terms & Conditions](#) and the [Ethical guidelines](#) still apply. In no event shall the Royal Society of Chemistry be held responsible for any errors or omissions in this *Accepted Manuscript* or any consequences arising from the use of any information it contains.

Micropatterned biofilm formations by laminar flow-templating

N. B. Aznaveh,^a M. Safdar,^{a,b} G. Wolfaardt^c and J. Greener^{*a}

We present a microfluidic device capable of patterning linear biofilm formations using a flow templating approach. We describe the design considerations and fabrication methodology of a two level flow-templating micro-bioreactor (FT- μ BR), which generates a biofilm growth stream surrounded on 3 sides by a growth inhibiting confinement stream. Through a combination of experiments and simulations we comprehensively evaluate and exploit control parameters to manipulate the biofilm growth template stream dimensions. The FT- μ BR is then used to grow biofilm patterns with controllable dimensions. A proof-of-principle study using the device demonstrates its utility in conducting biofilm growth rate measurements under different shear stress environments. This opens the way for quantitative studies into the effects of the local shear environment on biofilm properties and for the synthesis of a new generation of functional biomaterials with controllable properties.



ARTICLE

Micropatterned biofilm formations by laminar flow-templating

Cite this: DOI: 10.1039/x0xx00000x

N. B. Aznaveh,^a M. Safdar,^{a,b} G. Wolfaardt^c and J. Greener^{*a}

Received 00th January 2012,
Accepted 00th January 2012

DOI: 10.1039/x0xx00000x

www.rsc.org/

We present a microfluidic device capable of patterning linear biofilm formations using a flow templating approach. We describe the design considerations and fabrication methodology of a two level flow-templating micro-bioreactor (FT- μ BR), which generates a biofilm growth stream surrounded on 3 sides by a growth inhibiting confinement stream. Through a combination of experiments and simulations we comprehensively evaluate and exploit control parameters to manipulate the biofilm growth template stream dimensions. The FT- μ BR is then used to grow biofilm patterns with controllable dimensions. A proof-of-principle study using the device demonstrates its utility in conducting biofilm growth rate measurements under different shear stress environments. This opens the way for quantitative studies into the effects of the local shear environment on biofilm properties and for the synthesis of a new generation of functional biomaterials with controllable properties.

Introduction

Biofilms are inherently complex and heterogeneous living materials, with properties that change in space and time. In this sense, biofilms are among the most interesting and challenging materials to study analytically.^{1,2} While great advances have been made in the understanding of biofilms from the perspective of molecular biology in the last 5-10 years, there is a growing need for quantitative characterisation under well-defined physical conditions. This has prompted new creative approaches to characterisation, such as combined use of confocal laser scanning microscopy and fluorescence correlation spectroscopy for the study of growth and diffusion within the biofilm matrix² and flexible flow cells for the estimation of biofilm mechanical properties.³ Nevertheless there is a need for a versatile platform that enables both simple and quantitative *in situ* measurements of biofilms using standard laboratory equipment, while achieving strict control over the hydrodynamic environment. Optically transparent microfluidic (MF) channels are ideal environments to manipulate and study biofilms because they can achieve excellent control over hydrodynamic, chemical and thermal conditions and are readily examined by regular optical microscopes. In addition, a major practical advantage includes strongly reduced requirements on growth medium volumes. This opens the way for studies that require high fluid velocities and long-duration experiments, without compromise of growth media sterility when filling or replacing reservoirs. Recently, several manuscripts have been published on the use of

microfluidics to control hydrodynamics in low Reynolds number environments while studying its effect on biofilm morphology, mechanical properties, adsorption/detachment, efficacy of anti-fouling surfaces, streamer formation and planktonic cell proliferation.³⁻¹³ The current approach to growing biofilms in MF channels is to inoculate the entire microchannel, thereby exposing bacteria to the all wall surfaces. However, corner effects in rectangular microchannels result in variances in biofilm properties due to large differences between the values of wall shear stresses at the channel corners versus those at straight wall segments. In addition, recent work shows that biofilm overgrowth can strongly affect the free volume in MF channels, resulting in unpredictable changes to the hydrodynamic environment, thereby undermining the major advantage of MFs.^{12,13} Factors such as nutrient source and concentration have only limited impact on biofilm thickness and density, therefore a new approach to localise and limit biofilm growth in the microchannel is required.¹⁴

This work describes the development and demonstrates the functionality of a micro bioreactor that can overcome the problems above by confining biofilm growth to a region of the MF channel that experiences uniform wall shear stress. This was accomplished by generating co-flowing streams with controllable dimensions that geometrically localise biofilm growth on one microchannel wall and prevent growth in microchannel corners. Resulting biofilms are predicted to have more uniform dimensions, density, and bioactivity compared to those growing in heterogeneous hydrodynamic environments.¹⁶

The flow-templated micro bioreactor (FT- μ BR), presented here, brings specific design and operational enhancements over a co-flow device that we recently used for surface enhanced Raman studies of liquid streams.¹⁵ To the best of our knowledge, the FT- μ BR enables, for the first time, patterning of biofilms with controllable dimensions on a single microchannel wall. The biofilms were grown on the wall opposite a coverslip sealing layer to enable unobstructed inspection of the entire channel volume, including the cultured biofilms. Quantitative analysis was conducted using a normal bright field microscope with validation being provided by numerical simulation. In this work, we analysed the flow-template stream width and height to define and comprehensively explore reactor design features and operational control parameters. We used the FT- μ BR for a proof-of-principle study of the biofilm growth rate under different shear stress environments. This work demonstrates the utility of liquid-phase biofilm growth templating to enable accurate studies related to growth in different hydrodynamic environments. It also opens the way for optimising biofilm properties for new uses as functional materials.

Experimental

Materials and equipment

Syringe pumps (PHD 2000, Harvard Apparatus, Holliston, MA, USA) were used to inject liquids into the FT- μ BR inlets. Connective tubing was made of perfluoroalkoxy (PFA) with outer diameter 1.6 mm (U-1148, IDEX, WA, USA), which was connected to 60mL syringes (BD Scientific, NJ, USA) *via* connector assembly (P-200x, P-658, IDEX, WA, USA). Liquids were vacuum degassed before injection to minimise bubble formation on-chip. Sodium citrate was acquired from Sigma Aldrich and ultrapure water with resistivity of $18.1 \text{ M}\Omega\cdot\text{cm}^{-1}$ was used in the preparation of all solutions. Microfluidic device fabrication materials included polydimethyl siloxane (PDMS) (sylgard184, Dow corning, Canada) and glass cover slips (VWR, Mississauga, Canada). Optical micrographs of the biofilms were acquired using an inverted light microscope (Bruker, IX73, MA, USA) with fluorescence and white light transmission illumination. Biofilms were recorded at 2x magnification (numerical aperture 0.06) whereas high resolution images of bacteria were recorded at 100x magnification (numerical aperture 0.9). Images were collected using an uncooled, monochrome CCD camera (Lumenera Infinity 3-1, Ottawa, Canada). Imaging of green fluorescent protein (GFP) expressing bacteria was conducted on the same instrument using appropriate fluorescent excitation and filter cube.

Device Fabrication materials

The FT- μ BR channel features were fabricated by curing the uncrosslinked PDMS polymer against a silicon master mould (FlowJEM Inc., Toronto, Canada). Each level was fabricated separately before they were aligned and bonded. Bonding was achieved by exposing bonding surfaces to air plasma (PCD-001 Harrick Plasma, Ithaca, USA). The connection of inlets and outlets

were achieved using metal elbow capillaries that fit tightly into the punched inlets without the need for epoxy. The device was fully transparent, enabling optical characterisation.

Optical measurements

Optical densities and physical dimensions of template streams and the micropatterned biofilms were made using open access image analysis software (ImageJ V1.47). In all cases, background corrected images were first analysed along channel cross-sections for their pixel intensities. Often, an average cross-section profile was determined by averaging many profiles in the same vicinity. In order to avoid aberrations due to changes to ambient light levels, or low frequency oscillations in lamp brightness, background images were acquired regularly. For visualisation experiments of the template solution, calibration measurements were made with the channel completely filled with the dye solution (McCormick, London, Canada) and then the transparent confinement phase. The dye concentration was determined by adding 2 drops (measured gravimetrically to be approximately $50 \mu\text{L}$ per drop) per mL of nutrient solution and the limit of detection by *in situ* transmission microscopy was determined to be equivalent to 0.1 drops per mL. Estimation of the template stream vertical path length was made using Beer-Lambert law as discussed in the results section. The maximum and minimum pixel intensities within the channel filled with only clear confinement phase liquid and dye-containing liquid, respectively, were determined in advance to be $I_{\text{max}} = 2.88 \times 10^4$ (arb. units) and $I_{\text{min}} = 9.9 \times 10^{-3}$ (arb. units) using background corrected microscope images. In the case that regular background images were not attainable, for example during long-term biofilm growth experiments, normalisation was achieved using a segment of the image outside of the channel. The reduction in transmitted light as a result of biofilm development is expressed as optical density, which is defined here as the absorbance, analogous to the Beer-Lambert law. This definition of optical density has been shown previously to be proportional to biofilm mass.¹⁷ Automated colony counting using optical micrographs was accomplished using image analysis software as discussed in the Supplementary Information (Figure S6).

Computer simulations

All flow simulations were conducted in three-dimensions using COMSOL Multiphysics[®] software with a fine mesh and physics for laminar flow and transport of dilute species in an incompressible fluidic phase. Molecular diffusion of citrate molecules was simulated using diffusion co-efficient $D_{\text{citrate}} = 6.9 \times 10^{-10} \text{ m}^2\cdot\text{s}^{-1}$ and we used $D_{\text{dye}} = 2.0 \times 10^{-10} \text{ m}^2\cdot\text{s}^{-1}$ for the diffusion of water soluble dye molecules.¹⁸

Biofilm cultivation

The gram negative, rod-shaped motile bacterium *Pseudomonas sp.* strain CTO7 was selected for biofilm formation in the MF platform. We used a GFP expressing variant, CTO7-GFP.¹⁹ A pre-culture of planktonic *Pseudomonas sp.* was used as inoculum for biofilm formation. The suspended culture inoculum was obtained by shaking

the cultures of planktonic *Pseudomonas sp.* in 3 mL of 5 mM growth media at 300 rpm for 18 h at 30°C. Growth media was a modified AB type, consisting of 1.51 mM $(\text{NH}_4)_2\text{SO}_4$, 3.37 mM Na_2HPO_4 , 2.20 mM KH_2PO_4 , 179 mM NaCl, 0.1 mM $\text{MgCl}_2 \cdot 6\text{H}_2\text{O}$, 0.01 mM $\text{CaCl}_2 \cdot 2\text{H}_2\text{O}$ and 0.001 mM FeCl_3 with 10 mM Na-citrate $\cdot 6\text{H}_2\text{O}$ as the sole carbon source. The confinement phase consisted of the same ingredients as the growth media, but the Na-citrate concentration was 0 mM, which, therefore, did not support biofilm growth. Prior to inoculation, the MF system was disinfected with 70% ethanol for 2 h and then rinsing with sterile distilled water for 1 hour. Distilled water was displaced by flushing with sterile growth medium. Templated inoculation was conducted for 2 h. Due to the high surface area to volume ratio and due to the fact that the liquid residence time (30 s) was significantly shorter than the maximum specific planktonic growth time of *Pseudomonas sp.* CT07gfp, it was concluded that biofilm formation was strongly favoured over bacteria growth in the planktonic state.^{19,20} The GFP bacteria allowed imaging of the template inoculant stream by fluorescence microscopy (Fig. S2b). Following inoculation, growth media was templated along the same path as the inoculum. Visible biofilm formations were formed after approximately 20-40 h.

Reactor design

The FT- μ BR is shown schematically in Figure 1. Level 1 included a long measurement channel with length of $L_M = 32$ mm, width of $w_M = 2000$ μm , and a height of $h_M = 305$ μm . An inlet was punched at the upstream end of the measurement channel to introduce the confinement flow phase. Level 2 was aligned above Level 1 and included Inlet 2 for the introduction of the biofilm nutrient solution phase, such as bacteria-laden inoculant, growth media, or coloured liquid for visualisation experiments. The two levels were connected by a cylindrical junction hole that injected the biofilm nutrient solution phase into the measurement channel, where it encountered a flow of the confinement liquid, thereby templating biofilm growth. The biofilm templating stream width (w_T) and height (h_T) were tuned by changing the confinement flow rate and the template flow rate, Q_C and Q_T , respectively (Fig. 1b, c). In this paper we specify the flow rate ratio as Q_C/Q_T . The junction was fabricated by punching through the PDMS at known angle (θ) with a punch that yielded a known diameter (d) to better specify hydrodynamic flow conditions within the measurement channel. The measurement channel was sealed by a glass coverslip, which enabled observation of the template surface at the opposite microchannel wall using objectives that had working distances of at least 475 μm , the sum of the coverslip thickness and h_M . The device was placed cover slip down on an inverted microscope for imaging in transmission and fluorescence modes. The PDMS material is known to support gas diffusion, thereby eliminating concerns that O_2 depletion or CO_2 accumulation will impact biofilm respiration. Experiments were conducted in a temperature controlled room at $22^\circ \pm 2^\circ\text{C}$.

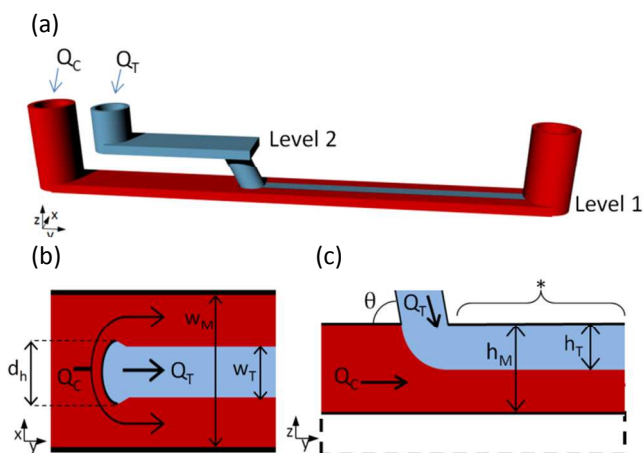


Fig. 1 (a) Schematic of the two-level device. The small channel in Level 2 (blue) brings the biofilm nutrient solution template stream to the measurement channel with flow rate Q_T . The inlet connected to the large (measurement) channel in Level 1 (red) brings the confinement solution with a flow rate of Q_C . Observation of the measurement channel occurs from the bottom side using an inverted microscope. (b) Schematic view of the cross-section in the y - x plane of the measurement channel with width $w_M = 2000$ μm . Junction diameter, d , was 450 μm , unless stated otherwise. Lateral confinement of biofilm template stream (blue) by the confinement stream (red) results in templated flow with width w_T . (c) Schematic view of the z - y cross-section of the measurement channel with height $h_M = 305$ μm and angle θ . Vertical confinement of biofilm template stream results in templated flow with height h_T . The biofilm nutrient solution template stream enters the measurement channel from the junction on the PDMS side of the channel. The bottom of the channel is sealed by a glass coverslip (dashed box) with thickness 170 μm . Biofilm cultivation occurs at the template surface (*).

In the Supplementary Information section, we use simulations to extensively explore the effect of the angle, θ , on flow template dimensions for different flow rate ratios (Figure S3). A competing effect between the $w_T|_0$ and $h_T|_0$ in the range $35^\circ > \theta > 90^\circ$ was noted. However, for $\theta < 45^\circ$ we noted a rapid increase in w_T . Since our goal was to maximise the confinement of the template stream in the vertical and horizontal dimensions, we chose the intermediate value of $\theta = 45^\circ$.

Results and discussion

Generating linear template flow patterns

The microchannel environment is well-suited for generating stable co-flowing streams of miscible liquids due to suppression of convective mixing.²¹ Upon emerging from the junction channel, the biofilm nutrient solution template stream continued to flow downstream, confined to the centre portion of the PDMS template surface in the measurement channel by the confinement stream. However, preliminary experiments attempting to generate stable template flow patterns demonstrated poor confinement of biofilm nutrient solution due to the interaction between highly diffusive small ions leaving the template solution and other template stream molecules, such as the carbon source (citrate; Fig S1a).¹⁸ We solved this problem by minimising the diffusion-driven flux of small molecules out of the biofilm nutrient solution template phase by eliminating their concentration gradients at the interface between the two streams, as discussed in the supplementary information. The effect was the strong reduction of mass-transfer between

confinement and template streams, resulting in a linear template solution with constant w_T (Fig S1b).

We used simulations and experiments to demonstrate the versatility in generating linear template flow patterns of biofilm nutrient solution with controllable dimensions. Computer simulations verified that after a few 10^2 's of microns downstream of the junction, the velocity and wall shear stress profiles were similar to those generated from a measurement channel with only one inlet (no junction) using a total flow rate equal to $Q_C + Q_T$. That is to say the segregated streams did not maintain memory of their initial upstream velocities. Figure 2a shows the results of a numerical simulation of the device presented here, which predicts that the shear stress (τ) along the templating wall was uniform within $\pm 2\%$ within the middle 1200 μm for the design discussed here. We used this information to determine the maximum limits on the width of the biofilm growth template solution. The co-flow patterns could also be modeled. Figure 2b shows the results of a typical simulation resulting in a template pattern, which could be used to predict details such as the shape, w_T and h_T of the template solution. As discussed in Supplementary Information we confirmed by experimentation and simulations that w_T and h_T were dependent on the flow rate ratio (Q_C/Q_T) only (Fig. S4), irrespective of the overall fluid velocity. This has the implication that the template stream dimensions can be produced using multiple Q_C and Q_T pairs, thereby opening the way for exploring the effect of applied shear force without affecting the footprint of patterned biofilm. Figures 2c and 2d show background subtracted images of the confined template flow streams passing through the microchannel at $Q_C/Q_T|_c = 1.67$ and $Q_C/Q_T|_d = 3.33$, respectively. Inspection of these images shows clearly that a decrease in template stream width was achieved from $w_{T,a} = 1064 \mu\text{m}$ to $w_{T,b} = 700 \mu\text{m}$.

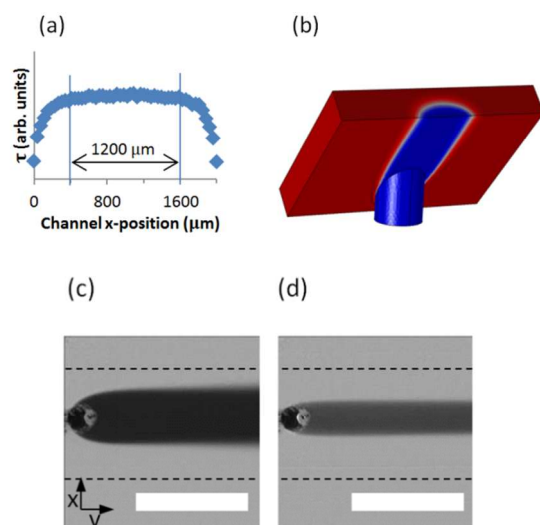


Fig. 2 (a) Shear stress (τ) profile along the templating wall for $Q_C = 2.5 \text{ mL}\cdot\text{h}^{-1}$, $Q_T = 0.6 \text{ mL}\cdot\text{h}^{-1}$. Vertical lines mark the region measuring approximately 1200 μm where τ is uniform within $\pm 2\%$. (b) Results from a three-dimensional numerical simulation showing isolation of a central template flow (blue) being supplied by volumetric flow rate of $Q_T = 0.6 \text{ mL}\cdot\text{h}^{-1}$ and a confinement flow (red) being supplied by a volumetric flow rate of $Q_C = 2.5 \text{ mL}\cdot\text{h}^{-1}$. The simulation is

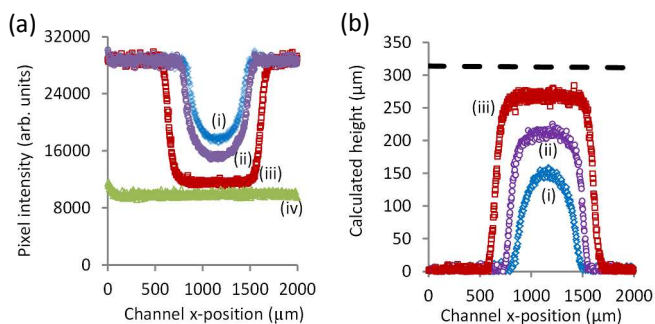
conducted in the first 1.5 mm after a junction with $d = 450 \mu\text{m}$ and $\theta = 45^\circ$. Background subtracted images of flow streams where (c) $Q_C = 0.5 \text{ mL}\cdot\text{h}^{-1}$, $Q_T = 0.3 \text{ mL}\cdot\text{h}^{-1}$ and (d) $Q_C = 1.0 \text{ mL}\cdot\text{h}^{-1}$, $Q_T = 0.3 \text{ mL}\cdot\text{h}^{-1}$. Dashed lines mark the channel walls which are invisible in background subtracted images. Scale bars in (c) and (d) are 2000 μm .

Quantitative measurement and control of flow templates

Quantitative pixel intensity profiles of the dye laden template streams were conducted at a number of flow rate ratios. Figure 3a shows results from 4 different flow rate ratios, $Q_C/Q_T =$ (i) 10, (ii) 3.33, (iii) 0.83, and (iv) 0, where the latter is the unconfined flow of a dye laden biofilm nutrient solution only. The pixel intensity reached its highest intensity, I_{max} , in vicinity of the confinement flow streams, where pixels were bright. The pixel intensity rapidly diminished at the interface between the confinement stream and the dye containing template flow stream. The value of w_T was determined to be 703 μm , 835 μm , 1240 μm for flow rate ratios (i), (ii) and (iii), respectively. The pixel intensity reached a local minimum in the centre of the template stream. Since diffusion-controlled mass-transfer between the template solution and the confinement solution was negligible, we concluded that the changes to the pixel intensity were due to the height of the template solution at various x-positions, h_x , not due to solution dilution. We made an estimation of h_x by applying the Beer-Lambert law (Eq. 1) to the data in the pixel intensity maps, assuming constant concentration, c ,

$$\log\left(\frac{I_x}{I_{\text{max}}}\right) = -a \cdot c \cdot h_x \quad (1)$$

where I_x is the local pixel intensity at the x-position along the channel cross-section, I_{max} is the intensity of the light passing through the channel containing only confinement-phase solution, and a is the dye solution absorptivity. With knowledge of the full channel height (305 μm), I_{min} and I_{max} we used Eq. 1 to determine $a \cdot c = 1.48 \times 10^{-3} (\mu\text{m}^{-1})$. Using this approach, we converted the raw pixel, I_x , intensity into an estimated height of the template flow solution at different positions along the channel cross-section. The maximum height at the centre of the template stream was taken as h_T . Three cross-section profiles are plotted in Figure 3b. For high values of Q_C/Q_T , we noticed that the peaks in h_x became “flattened” due to the resistance of the confinement fluid to deformation as it was compressed against the glass coverslip by the template solution. These plots allowed us to experimentally estimate w_T and h_T for different flow rate ratios. Figure 3c shows the variations in w_T and h_T with Q_C/Q_T and their comparison to simulation.



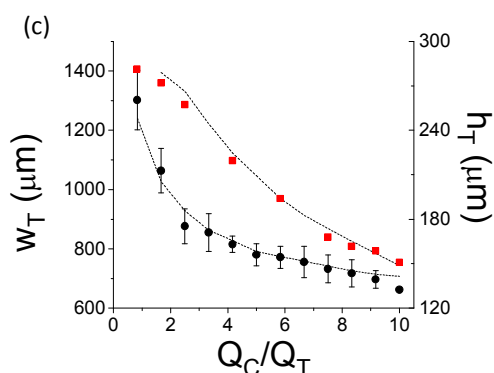


Fig. 3 (a) The results of measurements of the raw pixel intensity along the channel x-direction of dye laden template stream, (flow rate Q_T) being confined by a clear confinement stream (Flow rate Q_C) with flow rate ratios (Q_C/Q_T) of (i) 10, (ii) 3.33, (iii) 0.83, (iv) 0. Results for confinement liquid only ($Q_C/Q_T = \infty$) are not shown because they had the same values as l_{\max} . (b) Plot of h_T at different Q_C/Q_T values as calculated using Eq. 1 for 3 flow rate ratios (i), (ii) and (iii), in (a). The dashed line is the maximum channel height as calculated from Eq. 1 using l_{\min} shown in (a). Flow rate ratios in (a) and (b) were generated using constant $Q_C = 0.6 \text{ mL h}^{-1}$ and adjusting Q_T accordingly. (c) Changes to w_T (black circles) and h_T (red squares) with Q_C/Q_T for FT- μ BRs with $\theta = 45^\circ$ and $d = 450 \text{ }\mu\text{m}$. Error bars for w_T and h_T were generated by averaging the results from 3 separate experiments. Error bars for h_T are smaller than the data points. Results from simulations (dotted lines) using same conditions as the experiment, but diffusion is turned off to reduce computation time. Calculated heights using Beer-Lambert law. Maximum channel height (dashed line) was determined using (iv) in (a).

Templated growth of biofilms

We cultivated biofilms in the FT- μ BR at various values of Q_C/Q_T to demonstrate the ability to control the widths of patterned biofilm. Figures 4a,b show images of two biofilms acquired 50 h after inoculation, which were cultivated under the flow rate ratios $Q_C/Q_{T|a} = 3.33$ and $Q_C/Q_{T|b} = 1.67$.

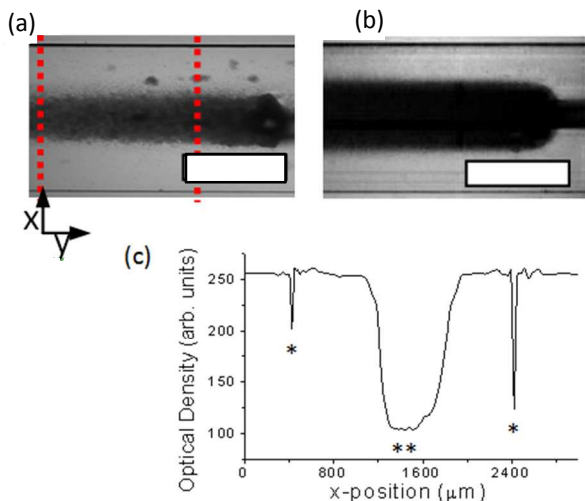


Fig. 4 Optical images of templated biofilms at $t = 50 \text{ h}$ after inoculation for flow rates: (a) $Q_C|_a = 1.0 \text{ mL h}^{-1}$, $Q_T|_a = 0.3 \text{ mL h}^{-1}$, (b) $Q_C|_b = 0.5 \text{ mL h}^{-1}$, $Q_T|_b = 0.3 \text{ mL h}^{-1}$. Average biofilm widths were: (a) $850 \text{ }\mu\text{m}$, (b) $1063 \text{ }\mu\text{m}$. Red dashed lines show the region between $800 \text{ }\mu\text{m} < y < 2300 \text{ }\mu\text{m}$. Flow in (a) and (b) was from right to left and scale bars are $1000 \text{ }\mu\text{m}$. (c) Average pixel intensity profile along the x-direction of the channel of the biofilm (***) shown in (a). Peaks marked with * show the channel walls. Base line correction was done to account for slight differential illumination across the channel. The curve was the average of multiple individual cross-sections generated between $800 \text{ }\mu\text{m} < y < 2300 \text{ }\mu\text{m}$.

We analysed their optical densities between $800 \text{ }\mu\text{m} < y < 2300 \text{ }\mu\text{m}$ after the junction to obtain an averaged cross-section profile of the biofilm (Figure 4c), which enabled accurate measurements of the biofilm width. Using this approach, the widths of the biofilms in Figures 4a and 4b were measured to be $850 \text{ }\mu\text{m}$ and $1063 \text{ }\mu\text{m}$, respectively. These values compared well with the measurements and simulations of the biofilm nutrient solution template width, w_T (Supplementary Information). Figure 5a shows an image of the entire measurement channel, which was stitched together from 4 separate images before background normalisation. The image of the biofilm was acquired 43 hours after inoculation under flow conditions $Q_C = 0.25 \text{ mL h}^{-1}$, $Q_T = 0.3 \text{ mL h}^{-1}$. Due to laminar flow and the resulting the low mass transfer of citrate molecules between the confinement and nutrient template streams, the template stream maintains good long-range patterning throughout the entire measurement channel, despite the low flow rate. We also note the progressive reduction in the optical density of the biofilm along the length of the measurement channel due to upstream nutrient depletion (Figure 5b). Given the channel cross-section area 0.61 mm^2 , the total flow velocity was calculated to be $v = 0.36 \text{ mm s}^{-1}$ and the maximum liquid residence time in the 12 mm templating region of the channel was approximately 30 s .

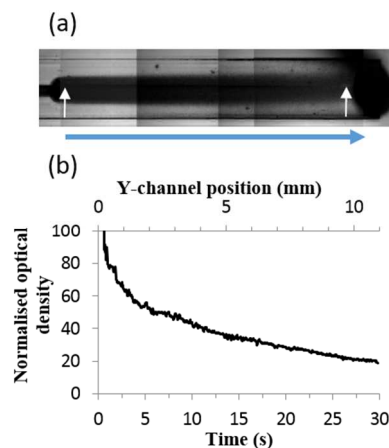


Fig. 5(a) Stitched image showing the complete measurement channel containing a biofilm 43 h after inoculation. Hydrodynamic growth conditions were $Q_C = 0.25 \text{ mL h}^{-1}$, $Q_T = 0.3 \text{ mL h}^{-1}$. White arrows mark the y_{\min} and y_{\max} for optical density measurements in (b). Blue arrow indicates the direction of flow was left to right. (b) Normalised optical density measurements based on x-averaged pixel intensity at different positions in the channel. The contact time between the nutrient solution and the biofilm is noted on the lower axis.

The resulting biofilm optical density, and therefore its mass density, decreased exponentially during the first 3 mm downstream of the junction, and then nearly linearly until the end of the channel. This suggests different mechanisms for citrate mass-transfer, for example rapid consumption near the biofilm/bulk liquid interface, leading to a depletion zone, and subsequent diffusion limited influx of citrate molecules into the depletion zone from the bulk liquid template stream. The FT- μ BR will be used in future studies to accurately investigate these questions and the role of the hydrodynamic environment on kinetics of citrate consumption.

Time dependant growth studies

Figure 6a shows time-series micrographs (i)-(vii) of flow-templated biofilms grown under flow conditions $Q_C = 1.0 \text{ mL}\cdot\text{h}^{-1}$, $Q_T = 0.3 \text{ mL}\cdot\text{h}^{-1}$ over the time interval $0 \text{ h} < t < 60 \text{ h}$. The process starts with the flow template inoculation of live bacteria, followed by culture under template flow of a biofilm nutrient solution (Figure 6(a)(i)). The biofilm growth initially consists of small disparate colonies within the flow template region (ii). Soon, these colonies begin a rapid expansion phase marked by colony growth and merging to form a continuous biofilm (iii)-(v). The images in this time interval reveal that there is a wide variance in the pixel intensity. Finally, the continuous biofilm becomes more uniform and opaque during a mature growth phase (vi)-(vii). Figure 6b shows quantitative measurements of the mean pixel intensity for a biofilm grown under flow conditions $Q_C = 0.5 \text{ mL}\cdot\text{h}^{-1}$, $Q_T = 0.3 \text{ mL}\cdot\text{h}^{-1}$. The standard deviation in their intensities was also calculated. We defined three key times in each pixel intensity curve: a slow growth phase during which micro colony formation is initiated, but does not strongly impact pixel intensity values, similar to the lag phase in batch cultures (*); a rapid growth phase with consequent increases in cell numbers and extracellular polymeric materials resulted in increased light scattering and rapid changes to pixel intensity (**); and a mature phase where biofilm cell growth, and potentially EPS (extracellular polymeric substances), is balanced by release from the biofilm (***) , resulting in near-constant pixel intensity. The results of a colony counting image analysis algorithm that was run on the same data set, demonstrated the relationship between the merging of biofilm colonies and the onset of the mature phase (Supplementary Information). We noted maximal values in the standard deviation of the pixel intensity near the curve inflection point, the point where the change in pixel intensity vs. time was greatest, likely because, asynchronous growth of differently sized biofilm colonies prior to colony merging into a confluent biofilm. The minimum standard deviation in the pixel intensity was observed when the biofilm had reached the mature phase. We note that the characterisation method employed here limits our ability to monitor the biofilm development after regions become opaque. Not all biofilms became opaque, and this effect could be mitigated, to a large degree, by changing exposure time or illumination intensity.

The FT- μ BR enabled comparative studies of biofilm growth under different flow conditions. Figure 6c shows changes to the normalised optical density for three different flow rates (i) $0.8 \text{ mL}\cdot\text{h}^{-1}$, (ii) $1.3 \text{ mL}\cdot\text{h}^{-1}$, (iii) $1.6 \text{ mL}\cdot\text{h}^{-1}$, which produced an applied shear stress against the growing biofilms of 17.4 mPa, 25.2 mPa, 29.8 mPa, respectively. The effect of increasing shear stress is noted in terms of two effects. The first effect observed with increasing wall shear stress is the difference in biofilm rate of growth during the rapid (exponential) growth phase. We estimated the rate of growth by measuring the slope of the optical density curves during the rapid growth phase, which is nearly linear. The results showed that biofilm rate of growth in this phase also increased linearly with the applied

wall shear stress (Supplementary Information, Fig. S7a). This is consistent with the fact that nutrient penetration into the biofilm *via* advection is influenced by hydrodynamic environment.²³ The second observable effect of increasing shear is that the time duration of the lag phase (t_{lp}) is longer. Lag phase is the time before measurable biofilm development occurred (similar to the lag phase in batch culture). As described elsewhere, this time was defined as the time between the end of inoculation ($t = 0 \text{ s}$) and when the tangent line of the maximum slope of the optical density curve intersected with the x-axis.²² We noted that t_{lp} varied linearly with the applied shear stress in the range of approximately 17 mPa to 30 mPa, with a slope of $1.9 \text{ h}\cdot\text{mPa}^{-1}$ (Supplementary Information Fig. S7b). A possible explanation for this observation is the reduced probability of cells to overcome the higher shear in order to successfully attach to the surface, which in turn leads to a longer time to reach the critical cell mass and EPS scaffolding needed for surface modification and biofilm proliferation. In Supplementary Information we use high resolution images of the bacteria to determine the growth and development of the adsorbed (pre-biofilm) bacterial layer during the lag phase.

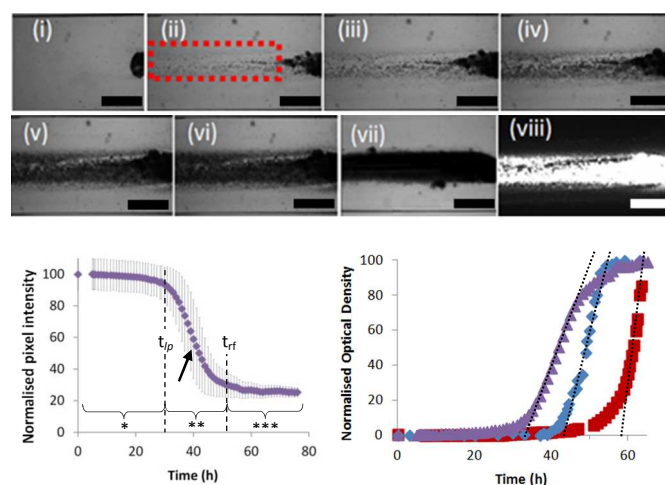


Fig. 6 (a) Images of the growing biofilm in the measurement channel at the times (i) 0 h, (ii) 37.0 h, (iii) 44.5 h, (iv) $t = 48.1 \text{ h}$, (v) $t = 49.8 \text{ h}$, (vi) $t = 51.0 \text{ h}$ and (vii) $t = 59.1 \text{ h}$ following inoculation. Flow conditions were $Q_C = 1.0 \text{ mL}\cdot\text{h}^{-1}$, $Q_T = 0.3 \text{ mL}\cdot\text{h}^{-1}$. The image (viii) is the fluorescent mode image of (vi), included here to demonstrate the potential to use fluorescent markers in future studies. Scale bars are 1000 μm . The red box in (ii) shows the area in which optical analysis took place for all images. Flow is from right to left. (b) Mean pixel intensities obtained within the red box in (a), showing the lag / adaptation phase (*), rapid growth (**) and mature phase with little or no net biofilm accumulation (***) . Flow conditions were $Q_C = 1.0 \text{ mL}\cdot\text{h}^{-1}$, $Q_T = 0.3 \text{ mL}\cdot\text{h}^{-1}$, flowing from right to left. The rapid growth phase starts at $t = t_{ri}$ and ends at time $t = t_{lp}$. The arrow points to an inflection in the curve where the rate of change of mean pixel intensity is the highest and the standard deviation in the pixel intensities is the greatest. Error bars give the standard deviation in the pixel intensities. (c) Time varying optical density measurements of biofilms grown under total flow rates $0.8 \text{ mL}\cdot\text{h}^{-1}$ (red squares), $1.3 \text{ mL}\cdot\text{h}^{-1}$ (blue circles), and $1.6 \text{ mL}\cdot\text{h}^{-1}$ (purple diamonds). Linear portions of the growth curves measured during the rapid growth phase highlighted with dotted lines. Error bars in (c) are excluded for clarity.

Conclusions

In this work we presented a microfluidic-based flow-templating bioreactor capable of localising biofilm formations to linear

patterns with specified dimensions, thereby avoiding growth in the channel corners and preventing channel constrictions due to overgrowth. The effect of reactor design on the template stream dimensions was carefully considered by experiment and simulation. The width and height of the template stream could be controlled by the flow rates of the biofilm nutrient solution and the confinement solution, enabling patterns of biofilm patterns with sizes as required. Proof-of-principle experiments were conducted demonstrating growth of biofilm formations with variable widths and biofilm growth kinetics studies. Using a regular transmission light microscope, the FT- μ BR can be a very useful platform for further studies into fundamental biofilm properties, such as lag times and growth rates for different bacteria under varying conditions. In addition, the ability to physically pattern biofilms with more homogeneous properties has the potential to benefit research into new biofilm-based functional materials.

Further developments could include the use new fabrication methods, such as laser cutting, to make junction holes with precise dimensions; isolation of inoculum and nutrient solution inlet channels to avoid biofilm growth upstream of the flow templating region; and the use of non-gas permeable device materials to better isolate the culture environment. In addition, the use of tracer particles such as fluorescent micro-beads can help with the characterisation of the effect of the biofilm patterns on the hydrodynamic environment in the channel can help with long-term control of biofilm formations.

Acknowledgements

The authors would like to thank Fonds de recherche du Québec – Nature et technologies (FRQNT).

Notes and references

^a Département de Chimie, Université Laval, 1045 Avenue de la Médecine, Québec, QC G1V 0A6, Canada.

^b Department of Chemistry, University of Eastern Finland, Yliopistokatu 7, FI-80101 Joensuu, Finland.

^c Department of Chemistry and Biology, Ryerson University, 350 Victoria Street, Toronto, ON, M5B 2K3, Canada, and Department of Microbiology, Stellenbosch University, Private Bag X1, Stellenbosch, 7602, South Africa.

Electronic Supplementary Information (ESI) available. See

DOI: 10.1039/b000000x/

1. S. Haruta, T. Yoshida, Y. Aoi, K. Kaneko and H. Futamata, *Microbes Environ.*, 2013, **28**, 285-294.
2. T. O. Peulen and K. J. Wilkinson, *Environ. Sci. Technol.*, 2011, **45**, 3367-3373.
3. D. N. Hohne, J. G. Younger, M. J. Solomon, *Langmuir*, 2009, **25**, 7743-7751.
4. M. Salta, L. Capretto, D. Carugo, J. A. Wharton, K. R. Stokes, *Biomicrofluidics*, 2013, **7**, 064118.
5. J.-H. Lee, J. B. Kaplan, W. Y. Lee, *Biomed Microdevices*, 2008, **10**, 489-498.
6. L. Richter, C. Stepper, A. Mak, A. Reinthaler, R. Heer, M. Kast, H. Bruckl and P. Ertl, *Lab Chip*, 2007, **7**, 1723-1731.
7. A. Valiei, A. Kumar, P. P. Mukherjee, Y. Liu and T. Thundat, *Lab Chip*, 2012, **12**, 5133-5137.
8. M. Skolimowski, M. W. Nielsen, J. Emneus, S. Molin, R. Taboryski, C. Sternberg, M. Dufva and O. Geschke, *Lab Chip*, 2010, **10**, 2162-2169.
9. H. Hou, L. Li, C. Ü. Ceylan, A. Haynes, J. Cope, H. H. Wilkinson, C. Erbay, P. de Figueiredo and A. Han, *Lab Chip*, 2012, **12**, 4151-4159.
10. E. Bester, G. Wolfaardt, N. Aznaveh and J. Greener, *Int. J. Mol. Sci.*, 2013, **14**, 21965-21982.
11. J. L. Song, K. H. Au, K. T. Huynh and A. I. Packman, *Biotechnol. Bioeng.*, 2014, **111**, 597-607.
12. J. Kim, H. S. Kim, S. Han, J. Y. Lee, J. E. Oh, S. Chung and H. D. Park, *Lab Chip*, 2013, **13**, 1846-1849.
13. K. Drescher, Y. Shen, B. L. Bassler and H. A. Stone, *P. Natl. Acad. Sci. USA*, 2013, **110**, 4345-4350.
14. G. Wolfaardt, J. Lawrence, R. Robarts, S. Caldwell and D. Caldwell, *Appl. Environ. Microbiol.*, 1994, **60**, 434-446.
15. F. Paquet-Mercier, N. Aznaveh, M. Safdar and J. Greener, *Sensors*, 2013, **13**, 14714-14727.
16. Y. Liu and J. H. Tay, *Water Res.*, 2002, **36**, 1653-1665.
17. R. Bakke, R. Kommedal and S. Kalvenes, *J. Microbiol. Methods*, 2001, **44**, 13-26.
18. E. L. Cussler, *Diffusion: Mass transfer in fluid systems*, Cambridge University Press, New York, 2007.
19. E. Bester, O. Kroukamp, G. M. Wolfaardt, L. Boonzaaier and S. N. Liss, *Appl. Environ. Microbiol.*, 2010, **76**, 1189-1197.
20. R. Bakke and P. Q. Olsson, *J. Microbiol. Methods*, 1986, **5**, 93-98.
21. H. A. Stone, A. D. Stroock and A. Ajdari, *Annu Rev. Fluid Mech.*, 2004, **36**, 381-411.
22. O. Kroukamp, R. G. Dumitrache, G. M. Wolfaardt, *Appl. Environ. Microbiol.*, 2010, **76**, 6025-6031.
23. H.J. Eberl, C. Picioreanu, J.J. Heijnen, M.C.M. van Loosdrecht, *Chem. Eng. Sci.*, 2000, **55**, 6209-6222.